*Andrzej Romanowski**

Magnetic Field in deviating Coils of the analysing Microscope

Magnetic field in the deviating doublet coils (DD) has been discussed; the system is applied to Roentgen analyzers, analyzing microscopes etc. The functions $H_0(z)$ and $H_2(z)$ for the deviating coils (DD) which allow to perform an analysis of the properties of electrooptical systems have been determined.

1. Introduction

Transversal sizes of an electron microbeam in the working plane of the scanning beam devices depend mainly on the deviation errors of the deviating systems and on the aberrations of focussing lenses. The third order deviation errors of the deviating systems depend, in turn, on the functions $H_2(z)$ and $V_2(z)$ [1, 2].

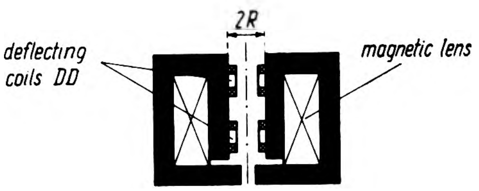

Fig. 1. A scheme of the objective lens of DD

The aberrations of the focussing lenses in the microbeam devices are determined by the objective lens aberrations. The latter may be diminished by applying the deviating doublet (DD). The DD coils are located inside the aperture of the objective lens hausing (see Fig. 1) [3].

2. Analysis of the functions $H_0(z)$ and $H_2(z)$ for the line coils of deviating system

Deviation of the electron beam in an arbitrary direction is controlled by the field produced in both the line deviating coils (horizontal deviation) and frame (vertical deviation). The scheme of the deviating system composed of the deviating coils of saddle type is presented in Fig. 2. The deviating currents of the line coils and frame are denoted by I_H and I_V,

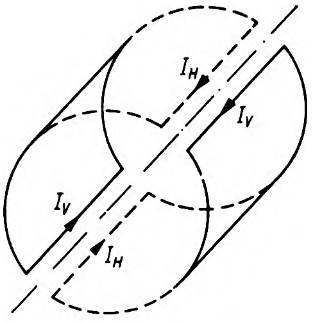

Fig. 2. Deflecting system

respectively. A cross-section of the single-loop deviating line coil DD with the masked quantities characteristic of deviating coils is shown in Fig. 3.

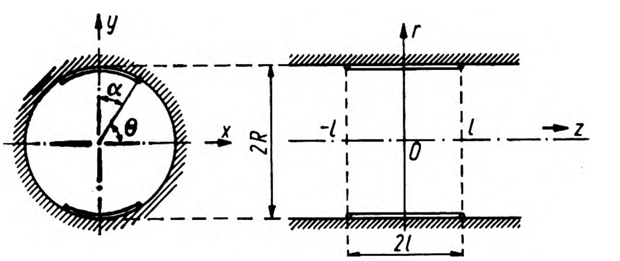

Fig. 3. Coils of line of the deflecting system DD

The symmetry conditions for the line coils given in Fig. 3 are defined by the formula [2]

$$\begin{aligned} H_x(x, y) &= -H_x(-x, y) = -H_x(x, -y), \\ H_y(x, y) &= H_y(-x, y) = H_y(x, -y), \\ H_z(x, y) &= H_z(-x, y) = -H_z(x, -y), \end{aligned} \tag{1}$$

where H_x, H_y and H_z are the components of the field strength vector $\boldsymbol{H}$. An analysis of the deviating field in the saddle coils, based on Bio-Savart Law, has been made by HAANTJES and LUBBEN [4]. However, their method can not be applied to the field analysis in the DD coils, because it does not take account of the influence of the screening coat of the magnetic

* Institute of Molecular Physics, Polish Academy of Sciences, Poznań, Poland.

lens. The presence of the magnetic screen changes considerably the field distribution in the deviating coils, affecting in particular the function $H_2(z)$.

In the present consideration the following assumptions have been accepted:

a) the lens coat is "ideally" magnetic ($\mu_r \to \infty$)

b) the internal aperture of the lens, in which the DD coils are located, is infinitely long.

Magnetic field in the deviating coils is described by the scalar Laplace equation

$$\Delta \Psi = 0, \tag{2}$$

where Ψ is the scalar magnetic potential for which

$$\boldsymbol{H} = -\operatorname{grad} \Psi \tag{3}$$

holds.

On the base of Fig. 3 and by virtue of the Amper Law $\Phi_L \boldsymbol{H} d\boldsymbol{l} = NI$ the boundary conditions in the cylindric coordinates r, φ, z, for $r = R$ take the form

$$\Psi = \begin{cases} NI \text{ for } \theta \leqslant \varphi \leqslant \theta + 2\alpha, \; |z| \leqslant 1, \; r = R, \\ -NI \;\; \pi + \theta \leqslant \varphi \leqslant \pi + \theta + 2\alpha, \; |z| \leqslant 1, \\ \qquad\qquad\qquad\qquad r = R, \\ 0 \qquad z \notin \langle -1, 1 \rangle, \; r = R, \end{cases} \tag{4}$$

where N denotes the number of coils in the deviating coil.

Magnetic potential Ψ for $r = R$ and $|z| \leqslant 1$ is given in Fig. 4. The solution of internal Dirichlet problem (2) and (4) is discussed in Appendix I. After substitution of (I.11) for (I.8) the solution takes the form

$$\Psi(r, \varphi, z) = \frac{8}{\pi^2} NI \sum_{n=1}^{\infty} \frac{1}{n} \sin n\pi/2 \sin n\alpha \times$$
$$\times \sin n\varphi \int_0^\infty \frac{I_n(kr) \sin kl \cos kz}{k I_n(kR)} dk, \tag{5}$$

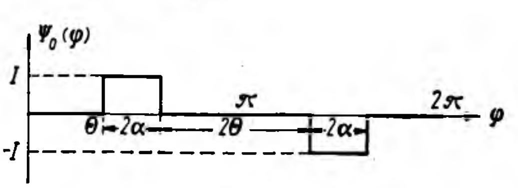

Fig. 4. Graph of the function $\Psi_0(\varphi) = \Psi(R, \varphi, z)$ for $|z| \leqslant l$

where $I_n(kr)$ denotes a modified Bessel function of the n-th order. In presence of (II.2) and (II.3) the functions

$$H_0 = (H_y)_{x=y=0} \text{ and } H_2 = \frac{1}{2!} \left(\frac{\partial^2 H_y}{\partial x^2} \right)_{x=y=0}$$

are

$$H_0(z) = -\frac{4}{\pi^2} NI \cos\theta \int_0^\infty \frac{\sin kl \cos kz}{I_1(kR)} dk, \tag{6a}$$

$$H_2(z) = -\frac{NI}{\pi^2} \left[\frac{\cos\theta}{2} \int_0^\infty \frac{k^2 \sin kl \cos kz}{I_1(kR)} dk + \right.$$
$$\left. + \cos 3\theta \int_0^\infty \frac{k^2 \sin kl \cos kz}{I_3(kR)} dk \right]. \tag{6b}$$

The functions appearing in formulae (6) being not elementary the respective numerical methods have been used for their evaluation. The calculations have been performed for the coils $2l = 20$, 25, 30, 35 and 40 mm long and for the internal aperture radius of the objective lens $R = 30$ mm. The results have been shown in Figs. 5,6,8 and 9. Fig. 5 presents the functions

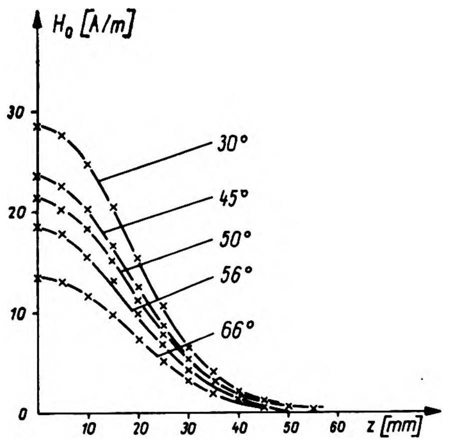

Fig. 5. Field strength distribution $H_0(z)$ on the axis for the coil of 35 mm length for different angles θ

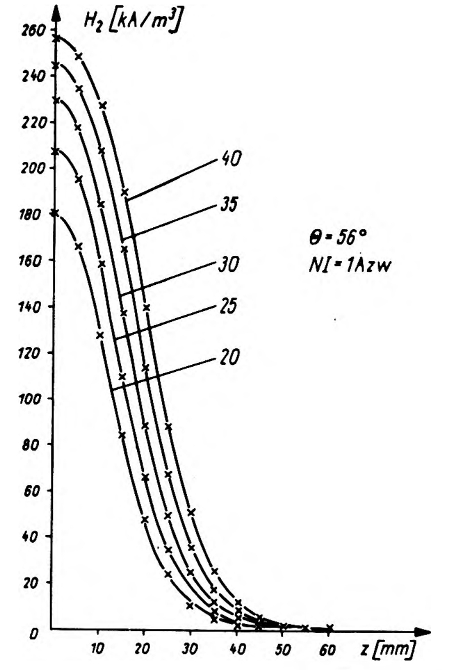

Fig. 6. Field strength distribution $H_0(z)$ for coils of various lengths for $\theta = 56°$

$H_0(z)$ in A/m for the coils 35 mm long and for the angles 30°, 45°, 50°, 56° and 66°. In Fig. 6 the function $H_0(z)$ has been shown for the angle $\theta = 56°$ and the coils of lengths 20, ..., 40 mm. From these graphs it follows that the length $2l$ of deviating coils influences the width of the distribution curve, while the angle θ determines the maximum value of the field strength H_0 on the axis. The graphs of the magnetic induction $B_0(z)$ in Fig. 7 are

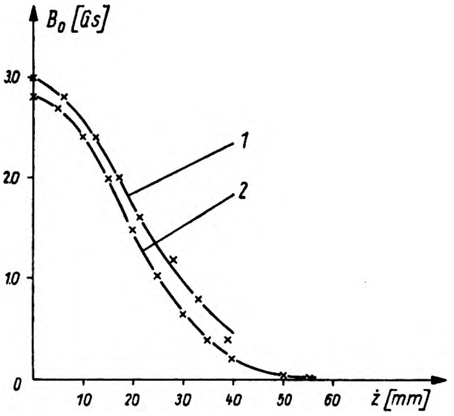

Fig. 7. Magnetic induction distribution on the axis $2l = 35$ mm, $\theta = 56°$
1 — on experimental curve, 2 — a curve computed on the base of formula (6a)

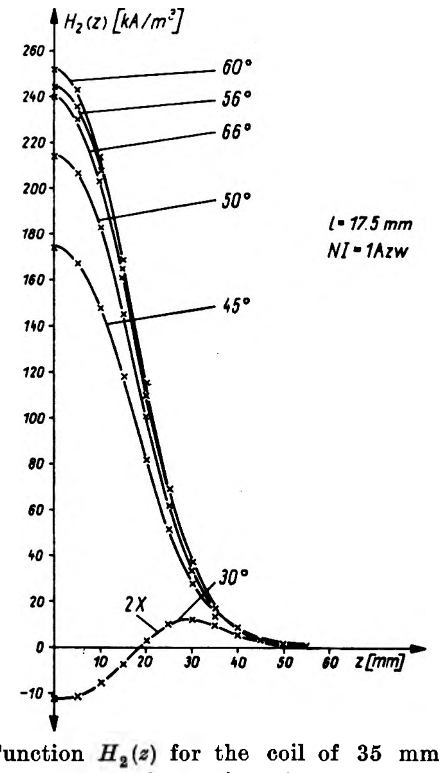

Fig. 8. Function $H_2(z)$ for the coil of 35 mm length for various θ

given for following parameters of the deviating coils: length = 35 mm, $\theta = 56°$, $N = 40$ coils and the deviating current 300 mA. The curve (1) was obtained experimentally with the help

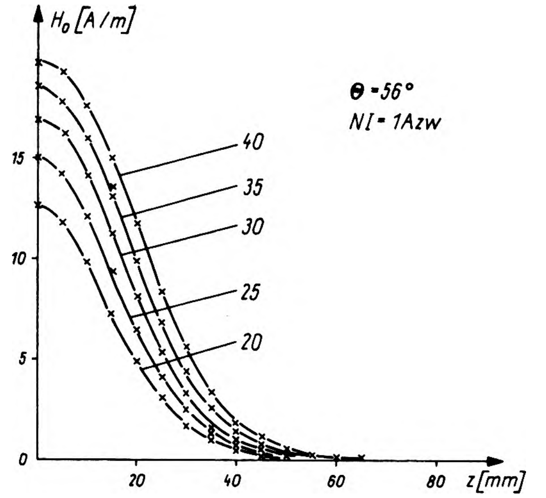

Fig. 9. Function $H_2(x)$ for coils of various length for $\theta = 56°$

of a Hall probe, while the curve (2) was computed from the formula (6a). The field $B_0(z)$ was measured by using the coil of sizes described above and as screening housing applying a cylinder made of ferrite rings of the length 125 mm and internal diameter 60 mm. The graphs of the H_2 functions calculated from (6b) are presented in Figs 8 and 9. For great values of θ these functions take the form of a bell curve.

3. Concluding remarks

From Figs. 5 and 6 it follows, that the function $H_0(z)$ increases, with the decreasing angle θ and increasing length $2l$ of the deviating system. The increase in H_0 results in an increment in the deviating system sensitivity [2], while a decrement of the angle θ results in decrease of $H_2(z)$. The latter function takes the least value (as measured by its modulus) for the angle $\theta = 30°$. It should be noticed that the function $H_2(z)$ given in Fig. 8 is $2\times$ magnified. A further decreasing of θ yields in an increase of the function H_2 toward negative values. Hence, it follows that the third order deviating errors of the (DD) deviating system will be the smallest for $\theta = 30°$. Additionally, as it follows from Fig. 8 for $\theta = 30°$, the function H_2 approximates the function determined by Kaashoek [2] giving the least deviating errors i.e. distortion, astigmatism and coma.

*

* *

The author expresses his gratitude to Dr. Andrzej Mulak for valuable remarks in the course of writing this paper.

Appendix I

For the line coils and the scalar magnetic potential the conditions of symmetry (1) have the form

$$\Psi(x, y) = \Psi(-x, y) = -\Psi(x, -y). \qquad (I.1)$$

The plane $z = 0$ (see Fig. 3) is a plane of symmetry, hence

$$\Psi(x, y, z) = \Psi(x, y, -z). \qquad (I.2)$$

The Laplace's equation in the cylindrical coordinates takes the form

$$\frac{\partial^2\Psi}{\partial r^2}+\frac{1}{r}\frac{\partial\Psi}{\partial r}+\frac{1}{r^2}\frac{\partial^2\Psi}{\partial\varphi^2}+\frac{\partial^2\Psi}{\partial z^2} = 0. \qquad (I.3)$$

The solution of (I.3) may be obtained by the variable separation method

$$\Psi(r, \varphi, z) = R(r)\Phi(\varphi)Z(z). \qquad (I.4)$$

Inserting (I.4) into (I.3) [5] we have

$$\frac{R''}{R}+\frac{1}{r}\frac{R'}{R}+\frac{1}{r^2}\frac{\Phi''}{\Phi}+\frac{Z''}{Z} = 0$$

since $\Phi(\varphi) = \Phi(\varphi+2\pi)$, hence $\Phi''+n^2\Phi = 0$

$$\Phi(\varphi) = \mathrm{A}\cos n\varphi+\mathrm{B}\sin n\varphi. \qquad (I.5)$$

In view of

$$\lim_{z\to\pm\infty} \Psi(r, \varphi, z) = \mathrm{const},$$

it follows that

$$Z''+k^2Z = 0.$$
$$Z(z) = C\cos kz+D\sin kz. \qquad (I.6)$$

The component $R(r)$ is a solution of the Bessel equation [5]:

$$R''+\frac{1}{r}R'-\left(k^2+\frac{n^2}{r^2}\right)R = 0,$$

$$R(r) = E\cdot I_n(kr)+FK_n(kr). \qquad (I.7)$$

On the base of (I.1) and (I.2) $A = D = F = 0$. Hence

$$\Psi(r, \varphi, z) = AI_n(kr)\sin n\varphi\cos kz,$$

where $A = BCE$.

The case $n = 0$ is trivial, therefore $n\in N$ where $N = 1, 2, \ldots$ under assumption that k changes in a continuous way within the interval $\langle 0, \infty)$

$$\Psi = \sum_{n=1}^{\infty}\sin n\varphi\int_0^{\infty} A_n(k)I_n(kr)\cos kz\,dk. \qquad (I.8)$$

The expression (I.8) takes the form

$$\Psi = \int_0^{\infty} a(k)\cos kz\,dk, \qquad (I.9)$$

where

$$a(k) = \sum_{n=1}^{\infty} a_n\sin n\varphi. \qquad (I.10)$$

The right-hand Fourier transform inverse to that given by (I.9) for $r = R$ is

$$a(k)_R = \frac{2}{\pi}\int_0^{\infty}\Psi(R, \varphi, t)\cos kt\,dt = \frac{2}{\pi}k\Psi_0\sin kl,$$

$$(a_n)_R = \frac{2}{\pi}\int_0^{\pi} a(k)_R\sin n\varphi\,d\varphi = \frac{8NI\sin kl}{\pi^2 kn}\sin n\frac{\pi}{2}\sin n\alpha,$$

hence

$$A_n(k) = \frac{8NI}{\pi^2}\sin n\frac{\pi}{2}\frac{\sin kl\sin n\alpha}{knI_n(kR)}. \qquad (I.11)$$

Appendix II

The modified Bassel function in (I.8) may be represented as

$$I_n(kr) = \left(\frac{kr}{2}\right)^n Q_n(kr),$$

where

$$Q_n(kr) = \sum_{k=0}^{\infty}\frac{1}{k!(n+k)!}\left(\frac{kr}{2}\right)^{2k}. \qquad (II.1)$$

Hence, $I_1(kr)\sin\varphi = kQ_1y/2$, $I_3(kr)\sin 3\varphi = k^3Q_3y(3x^2-y^2)/8$. On the base of (3)

$$H_y = -\frac{\partial\Psi}{\partial y} = -\frac{8NI}{\pi^2}\left\{\frac{\sin\alpha}{2}\left[\int_0^{\infty} kQ_1dZ_1 + y\int_0^{\infty} k\frac{\partial Q_1}{\partial y}dZ_1\right]-\frac{\sin 3\alpha}{24}\left[-2y^2\int_0^{\infty} k^3Q_3dZ_3 + (3x^2-y^2)\int_0^{\infty} k^3Q_3dZ_3+(3x^2-y^2)\times y\int_0^{\infty} k^3\frac{\partial Q_3}{\partial y}dZ_3\right]+\ldots\right\}, \qquad (II.2)$$

where

$$dZ_n = \frac{\sin kl\cos kZ}{kI_n(kR)}dk.$$

In view of (II.1)

$$(Q_n)_{x=y=0} = 1,\ \left(\frac{\partial Q_n}{\partial x}\right)_{x=y=0} = \left(\frac{\partial Q_n}{\partial y}\right)_{x=y=0} = 0,$$
$$\left(\frac{\partial^2 Q_1}{\partial x^2}\right)_{x=y=0} = k^2/8. \qquad (II.3)$$

Магнитное поле в бобинах отклоняющего дублета анализирующего микроскопа

Обсуждено отклоняющее магнитное поле в бобинах отклоняющего дублета. Эта система применяется в рентгеновских анализаторах, анализирующих микроскопах и т. д. Приведены функции $H_0(z)$ и $H_2(z)$ для бобин дублета, позволяющих производить анализ электронооптических свойств системы.

References

[1] Haantjes I., Lubben G. I., *Errors of magnetic deflection I*, Philips Res. Rep. 12, 1957, pp. 46–68.

[2] Kaashoek J., *A study of magnetic-deflection errors*, Philips Res. Rep. Suppl. 11, 1966, pp. 1–113.

[3] Amboss K., Wolf E. D., *Double deflection aberrations in a scanning electron microscope*, Rec. of 11-th Symp. Electron, Ion, Laser Beam Technol., San Francisco Press, 1971.

[4] Haantjes I., Lubben G. I., *Errors of magnetic deflection II*, Philips Res. Rep. 14, 1959, pp. 65–97.

[5] Tichonov A. N., Samarskij A. A., *Uravnenia Matematicheskoy fizyki*, Moskva 1972.

Received, October 7, 1975